RSC Advances

PAPER

View Article Online
View Journal | View Issue

Cite this: *RSC Adv.*, 2016, **6**, 7302

Preparing electrochemical active hierarchically porous carbons for detecting nitrite in drinkable water†

Baojun Ding,[a] Hong Wang,[a] Shengyang Tao,*[a] Yuchao Wang[b] and Jieshan Qiu[c]

Received 22nd October 2015
Accepted 9th January 2016

DOI: 10.1039/c5ra22116a

www.rsc.org/advances

A class of hierarchically porous carbons were prepared by a facile dual-templating approach. The obtained samples were characterized by scanning electron microscopy, X-ray diffraction, Raman spectroscopy, Brunaner–Emmett–Teller measurement and electrochemical work station, respectively. The porous carbons could possess large specific surface area, interconnected pore structures, high conductivity and graphitizing degree. The resulting materials were used to prepare integrated modified electrodes. Based on the experimental results, the as-prepared hierarchically porous graphite (HPG) modified electrode showed the best electroactive performances toward the detection of nitrite with a detection limit of 8.1×10^{-3} mM. This HPG electrode was also repeatable and stable for 6 weeks. Moreover, this electrode was used for the determination of nitrite in drinkable water, and had acceptable recoveries.

Introduction

Carbon is a widely used material in electrochemical applications.[1–6] Its different allotropes (amorphous, diamond, graphite, fullerenes, and nanotubes) exhibit distinct conductivities and morphologies.[7] Carbon materials can be made into lots of microtextures, such as fibers, powders, tubes, films, foams and hybrids,[8,9] which are suitable for various requirements. Due to the stable chemical and physical stability over a wide range of temperatures and solvents, carbon materials can retain reversibility properties in electrochemical redox reactions, even in very fast charge transfer processes.[10–14] The performance of carbon electrodes depends on several factors, such as the surface area, porosity and conductivity of materials.[15] The hybridization of carbon atoms directly determines all these material features.

Because of the large surface area and tunable pore structure, porous carbon materials have attracted great interest from electrochemists.[16,17] The adsorption of active molecules on the electrode can be significantly enhanced by the pores. This feature is in favor of surface redox reactions. Active carbons were firstly used as porous carbon electrodes since they have a huge surface area and are easy to obtain.[18] However, the pore size in the active carbon is usually too small for molecules diffusion. To overcome this shortage, hierarchically porous carbons were developed. Macropores serving as ion-buffering reservoirs can minimize the diffusion distances. Mesopores can decrease ion-transport resistance. Micropores are capable of selecting the size and shape of molecule and increasing the interactions between molecules and electrodes.[19–21] In spite of this, most hierarchically porous carbons are in the amorphous form. The conductivity of them is also not satisfied because these carbons contain a mixture of tetrahedral (sp^3) and trigonal (sp^2) carbon hybridization.[22] Nowadays, carbon nanotubes (CNT) and graphene, which are nanomaterials of sp^2-bonded carbon, are widely adopted to fabricate carbon electrodes,[23–28] owing to their good conductivity. Nevertheless, the small surface area, expensive price and cumbersome preparations limit their applications. Therefore, developing a kind of carbon materials with hierarchically porous structure and ideal conductivity will be important for the electrochemical research.

Recently, we reported the preparation of highly graphitized porous carbon monoliths.[29] This kind of materials have the benefits of both a porous structure and degree of graphitization. As well known, graphite consists of parallel stacking of two-dimensional (2D) graphene layers and has a high conductivity.[30] So the graphitized hierarchically porous carbon should be an excellent material for electrodes. Herein, we studied the electrochemical properties of the highly graphitized porous carbon and its sensing ability to nitrites in water. As an important water solubility pollutant, nitrites are highly carcinogenic to human beings. Moreover, nitrites are broadly added in food as preservatives. It can derive methemoglobin, which induces acute hypoxia in blood. Furthermore, when the nitrite

[a]*School of Chemistry, Dalian University of Technology, Dalian, Liaoning, P. R. China. E-mail: taosy@dlut.edu.cn; Fax: +86-411-84986035; Tel: +86-411-84986035*

[b]*Water Desalination and Reuse Center, Division of Biological and Environmental Science and Engineering, King Abdullah University of Science and Technology, Thuwal 23955-6900, Saudi Arabia*

[c]*Carbon Research Laboratory, Liaoning Key Lab for Energy Materials and Chemical Engineering, State Key Lab of Fine Chemicals, School of Chemical Engineering, Dalian University of Technology, Dalian, Liaoning, P. R. China*

† Electronic supplementary information (ESI) available. See DOI: 10.1039/c5ra22116a

reacts with amines and amides, it can be converted to *N*-nitrosoamines, which cause stomach cancer.[31–34] Detecting nitrites are quite necessary because they are highly toxic in biological systems. In this work, it was found that the graphitization degree, wettability and metal residue of the hierarchically porous carbon could affect its electrochemical performance. The porous carbon with the highest graphitization degree showed the best sensing ability to nitrites in water. The detection limit reached 8.1×10^{-3} mM, which is lower than the national life table-water standard.[35]

Experimental section

Materials

Tetramethoxysilane (TMOS) was bought from the Chemical Factory of Wuhan University (Wuhan, China). F127 (M_w = 12 600), phenol (AR), formaldehyde solution (formalin 37 wt%) and polyethylene glycol (PEG, M_w = 10 000) were obtained from Aladdin Chemical Co., Ltd. (Beijing, China). Sodium nitrite ($NaNO_2$) was supplied by Sigma-Aldrich. Nitric acid (AR) was purchased from Beijing Chemical Reagents Factory (Beijing, China). 25 wt% ammonia (AR), sodium hydroxide (AR), potassium chloride (AR), $FeCl_3 \cdot 6H_2O$ (AR), potassium ferricyanide (AR), hydrochloric acid (AR), acetic acid and absolute alcohol were purchased from Fuyu Fine Chemical of Tianjin Co., Ltd. (Tianjin, China). Other reagents were of analytical grade and used as received. All the reagents mentioned above were used without further purification.

Preparation of resol precursor

Typical method was used for the preparation of the soluble low-molecular-weight resol from phenol and formaldehyde in base.[36] 1.22 g (13 mmol) of phenol was melted at 40 °C, and 0.26 g (1.3 mmol) of 20% NaOH aqueous solution was added dropwise with stirring. About 10 min later, 1.05 g of formalin (37 wt%) containing formaldehyde (13.0 mmol) was added slowly at 75 °C and kept under stirring for 1 h. Cooled down to room temperature, the product was mixed with 0.6 M HCl solution in order to adjust the pH to neutral (about 7.0). The resultant resol was redissolved in ethanol for storage, after removing the water *via* rotary evaporation below 50 °C.

Preparation of hierarchically porous silica (HPS)

HPS was prepared according to the literature.[37,38] Firstly, 8.85 g polyethylene glycol (PEG, M_w = 10 000) was homogeneously dissolved in an aqueous solution of acetic acid (0.01 M). Subsequently TMOS (30 mL) was added and violently stirred for about 10 min for hydrolysis at 0 °C. Secondly, the semi-transparent solution was transferred into PE (poly ethylene) tubes. The PE tubes were sealed and kept at 40 °C for 12 h for gelation and then aged for about 24 h. Thirdly, the resultant wet gels were immersed into the 1.0 M aqueous solution of ammonia and refluxed for 9 h at 110 °C. Aqueous solution of nitric acid (0.1 M) was added to neutralize when the mixture cooled down to room temperature. The wet silica gels were evaporation-dried at 60 °C after repeated washing by deionized water, followed by calcination from room temperature to 650 °C with a heating rate of 5 °C min^{-1} and holding at 650 °C for 5 h in air in order to remove organic chemicals.

Preparation of hierarchically porous graphite with Fe doping (HPG-Fe)

In a typical synthesis,[29] tri-block copolymer F127 (1.0 g) was dissolved in ethanol (5 g). A certain amount of $FeCl_3 \cdot 6H_2O$ and resol (2.0 g) were in turn added under stirring at room temperature for 30 min. Then HPS (1.2 g) was immersed in the homogeneous solution under static conditions at 25 °C for 24 h, and an additional 24 h was taken to evaporate ethanol at 25 °C. Initial thermal-treatment was carried out by heating the dry materials at 100 °C to lead further polymerization of phenolic resols. In the process of pyrolysis, the resulting composite monoliths were calcined at 1200 °C for 6 h under nitrogen at a heating rate of 1 °C min^{-1} below 450 °C and 5 °C min^{-1} above 600 °C. After cooling to room temperature, the resultant black block was collected and washed with NaOH (2 M) aqueous solution to etch the silica. Immediately, the samples were washed with deionized water several times to remove the residuals. Finally, the products labeled as HPG-Fe were obtained after drying in an oven at 100 °C overnight. Elemental analysis (wt%): C, 63.14.

Preparation of hierarchically porous graphite (HPG)

The HPG was prepared based on previous work of preparing HPG-Fe. At first, HPG-Fe was immersed in HCl (1.0 M) solution to remove iron element. Then the solid sample was removed out and rinsed by water until pH = 7.0. Finally, the product was dried at 100 °C to obtain pure HPG. Elemental analysis (wt%): C, 94.06.

Preparation of sulfonated hierarchically porous graphite (HPGS)

At first, the appropriate amount of dried HPG was put into 50 mL of concentrated H_2SO_4 at 100 °C overnight. Then the products were washed with deionized water and dried at 100 °C to obtain the HPGS. Elemental analysis (wt%): C, 81.13; S, 1.60.

Preparation of hierarchically porous carbon (HPC)

The preparation of HPC was the same as HPG-Fe, except the soaking solution was not added $FeCl_3 \cdot 6H_2O$ and the carbonization temperature was 800 °C. Elemental analysis (wt%): C, 94.06.

Preparation of integrated electrodes

The performance of the as-prepared materials used as sensors was tested using a three-electrode system. The electrode surface was modified with the following procedure: first, the bare glassy carbon electrodes (GCE) were firstly polished to a mirror finish with 0.3 and 0.05 μm alumina slurry followed by thoroughly rinsing with deionized water. After sonicating successively in 1 : 1 nitric acid, ethanol and deionized water, the electrodes were rinsed with deionized water and was dried under the

stream of high purity argon for further use. In order to prepare the modified electrode, 1.0 mg porous carbon (HPG-Fe, HPG, HPGS or HPC) was dispersed in 1.0 mL of 0.1% (w/v) chitosan solution with ultrasonication for 2 h. With a microinjector, 5 μL of the suspension was dropped on the freshly prepared GCE surface and dried at room temperature. The resulting electrode was referred to as-prepared carbon electrode, where as-prepared carbon electrode means HPG-Fe, HPG, HPGS or HPC electrode.

Material characterization

The microscopic features of the samples were characterized by scanning electron microscopy (SEM, JSM-5600LV), X-ray diffraction (XRD) patterns were obtained on a Rigaku D/MAX-2400 X-ray powder diffractometer (Japan) using Cu Ka radiation, operating at 40 kV and 10 mA. (PORESIZER-9320, Micromeritics Co., USA). The nitrogen adsorption and desorption isotherms were measured at 77 K using an ASAP2010 analyzer. Before the measurements, samples were degassed under vacuum at 373 K overnight. The specific surface areas were calculated by the Brunauer–Emmett–Teller (BET) method and the pore size was calculated using the Barrett–Joyner–Halenda (BJH) model. Raman spectra were collected using a Nicolet Almega XR Raman system with a 532 nm excitation laser from Thermo Fisher Scientic Inc. Element contents were performed on 0.0001 mg/varioEL. A SL200B (Solon Tech. Inc., Ltd. Shanghai) contact-angle goniometer was used for static contact angle measurements.

Electrochemical measurement

All of the electrochemical experiments were performed using a Model CHI660E electrochemical workstation (CH Instruments, Inc., USA) with a conventional three-electrode cell, in which the bare or modified GCE (d = 3 mm), the saturated calomel electrode, and platinum wire served as the working electrode, reference electrode, and auxiliary electrode, respectively. Electrochemical impedance spectroscopy (EIS) analysis was carried out in 0.1 M KCl containing 5 mM $[Fe(CN)_6]^{3-}$/$[Fe(CN)_6]^{4-}$ in the frequency of 10^5 to 0.01 Hz with an amplitude of 5.0 mV under the open circuit potential. Differential Pulse Voltammetric (DPV) was used for the detection of $Fe(CN)_6^{3-}$ with the potential range of −0.2–0.7 V at the following parameters: pulse width, 0.0167 s; pulse period, 0.5 s; amplitude, 5 mV; and increment potential, 4 mV. The chronocoulometric study was used to obtain the surface excess. All the various drinkable water samples were filtered through a 0.22 μm membrane prior to detection. 1 mL sample containing 50 mM (or 5 mM) nitrite was mixed with 9 mL PBS (pH = 7) to determine nitrites by CV using the standard addition method. All of the solution was purged with stream of N_2 for 10 min and sealed under N_2 atmosphere.

Results and discussion

Material characterization

According to SEM images in Fig. 1, HPG-Fe, HPG and HPC showed three dimensional carbon skeleton with a number of

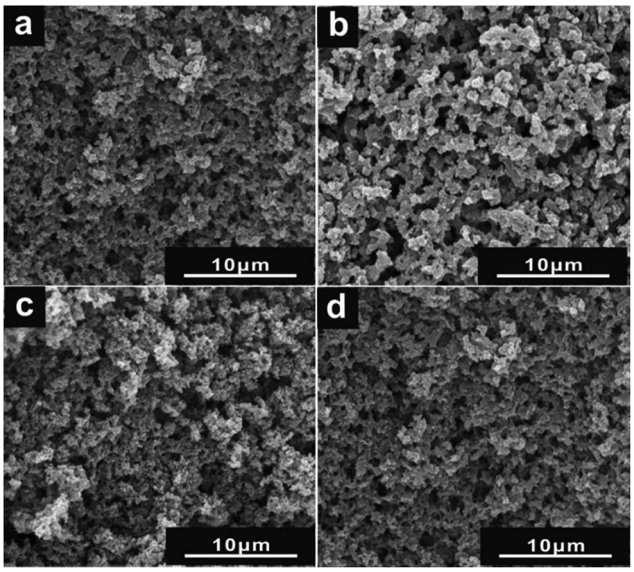

Fig. 1 SEM micrographs of carbon samples. (a) HPG-Fe, (b) HPG, (c) HPGS, (d) HPC.

macropores. These pores were interconnected to each other, forming continuous channels. The framework of HPG didn't collapse under the structure transformation from amorphous to graphitized, indicating that the HPS played an important role as support and protector. The HPG had a better pore structure than HPG-Fe, indicating that remove of Fe could expose more pores. HPGS exhibited a less porous structure than other materials. This may be caused by the sulfonated process. The carbon skeleton is partly destroyed.

The nitrogen adsorption-isotherms of the samples are shown in Fig. 2. The HPG-Fe, HPG, and HPGS showed a broad H2-type. Hysteresis loops covering a p/p_0 range of 0.45–0.96 indicate the existence of multi-size cylindrical mesopores. Table 1 summarizes the BET surface area values of different samples. Compared with HPG-Fe, the surface area of HPG was increased after removing the iron. Meanwhile, the surface area and pore diameter of HPGS were larger than HPG. This phenomenon

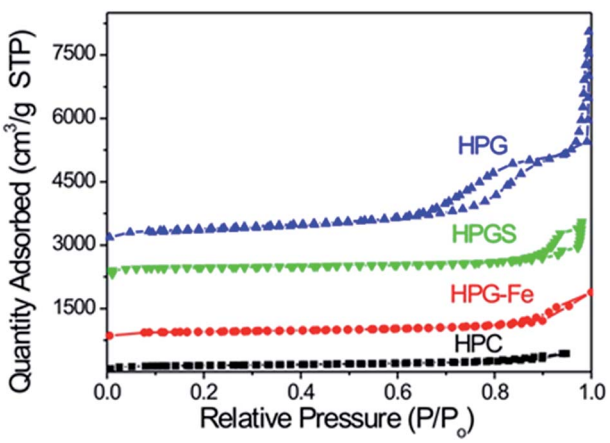

Fig. 2 N_2 adsorption–desorption isotherms of carbon samples.

Table 1 Pore structure parameters of the as-prepared materials

Sample	Surface area/ $m^2\ g^{-1}$	Pore diameter/ nm	Pore volume/ $cm^3\ g^{-1}$
HPG-Fe	485.66	11.58	0.56
HPG	507.47	15.93	1.07
HPGS	535.68	22.40	1.60
HPC	1067.43	10.20	0.98

may be due to the pores brought by the destruction of the carbon skeleton. The HPC presented highest surface area (1067.43 $m^2\ g^{-1}$) in the samples, because of the low degree of graphitization. Amorphous active carbon usually has a large surface area. All the mesopore sizes of these carbon materials are larger than 10 nm, which is big enough for the diffusion of ions in pores.

X-ray diffraction is used to explore the graphitization degree of materials. As shown in Fig. 3, the HPC did not exhibit a crystal structure and there is not obvious peak on the diffraction curve. The curve of HPG have two sharp characteristic peaks at 26° and 43°, which corresponded to the diffraction from (002) and (101) planes of graphite, respectively.[39] Such strong and narrow peaks mean a high graphitization degree of these carbon materials. The diffraction curve of HPG-Fe also showed a peak at 26° and some other peaks corresponding to the diffraction of iron. These peaks indicate the existence of iron. After sulphuric acid treatment, the peak at 26° of HPGS becomes weak and broad. It implies that the procedure of surface modification damages the ordered graphite structure.

Raman spectra of samples are shown in Fig. 4. The G-band, characteristic for graphitic materials, is located at 1568 m^{-1} and represents the vibration of the ideal graphite (E_{2g} symmetry). Other bands indicate a disordered graphitic lattice. The D_1 band (1340 cm^{-1}) represents the vibration of graphene layer edges (A_{1g} symmetry). The D_2 band (2714 cm^{-1}) is assigned to a few layers of graphene, the carbon wall is constituted by a few graphitic layers.[40] The HPG-Fe and HPG had a fine graphite structure. The G-band of HPGS decreased, indicating a decrease of the amount of graphitic carbon, as it had been confirmed previously by XRD analysis. The shape of the HPC's G-band was weak which means the lowness of the graphitization degree.

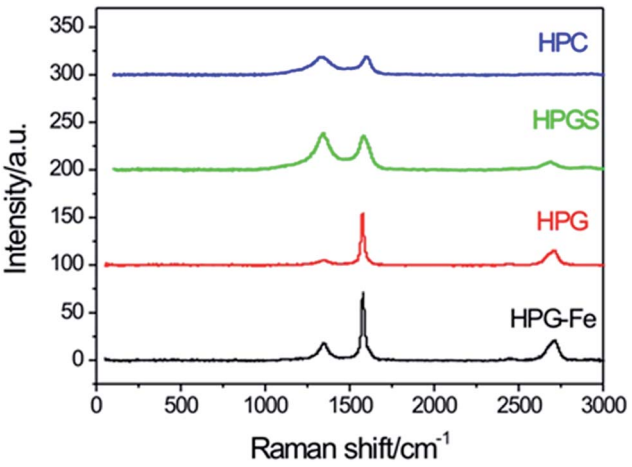

Fig. 4 Raman spectra of carbon samples.

The contact angles were tested to examine the surface wettability of the materials. HPG, HPG-Fe and HPC were all hydrophobic with the water contact angles between 121° and 131° (Fig. 5). HPGS had a smaller water contact angle, indicating the hydrophilic surface formed because of a large amount of hydroxyl groups on the surface (the images of the water contact angles was saw in Fig. S1, in the ESI†).

Electrochemical characterization of porous carbon electrodes

The electrochemical properties of different porous carbon modified electrodes were studied to find the one with the best performance to detect nitrite. First, CV and EIS experiments were performed to explore the conductivity and the electron-transfer process of the electrodes. Fig. 6A shows the CVs of the integrated hierarchically porous carbons electrodes in $Fe(CN)_6^{3-}$. The HPG electrode shows the best electron conductivity. The peak current of HPG electrode is stronger

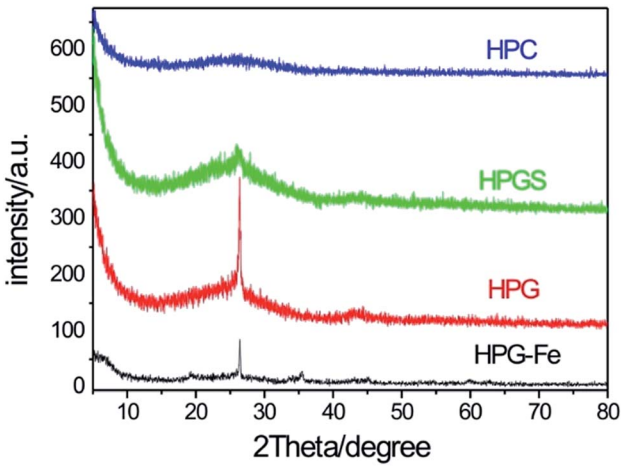

Fig. 3 XRD patterns of carbon samples.

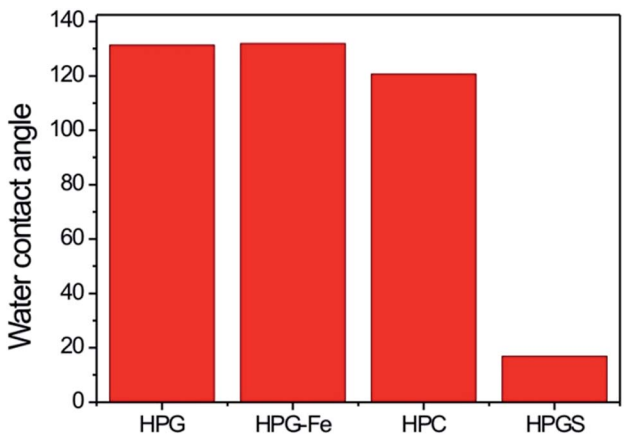

Fig. 5 The water contact angles of carbon samples.

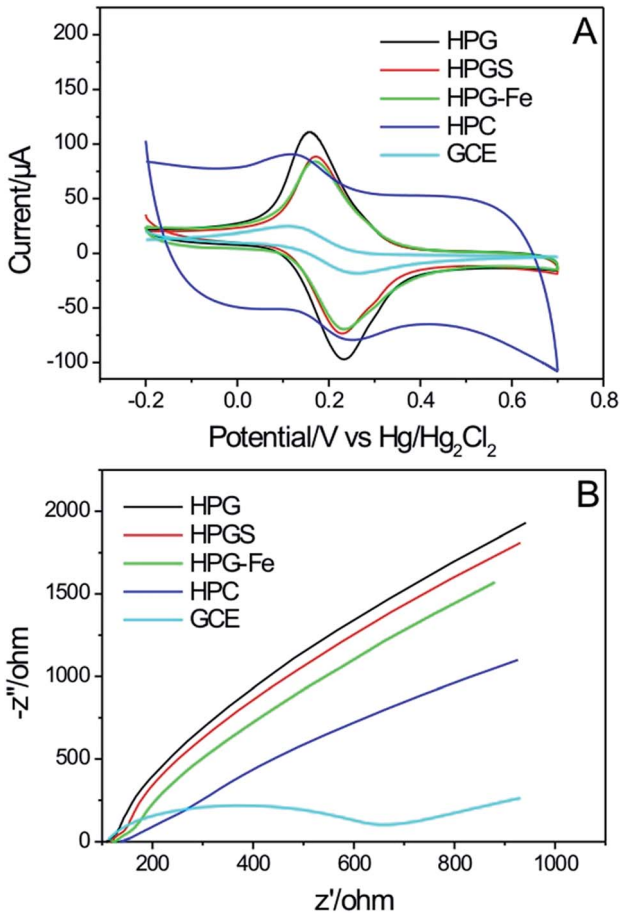

Fig. 6 (A) Cyclic voltammograms and (B) EIS spectra of HPG electrode, HPGS electrode, HPG-Fe electrode, HPC electrode, and bare GCE (the magnifying image of low Nyquist plot part was saw in Fig. S2, in the ESI†).

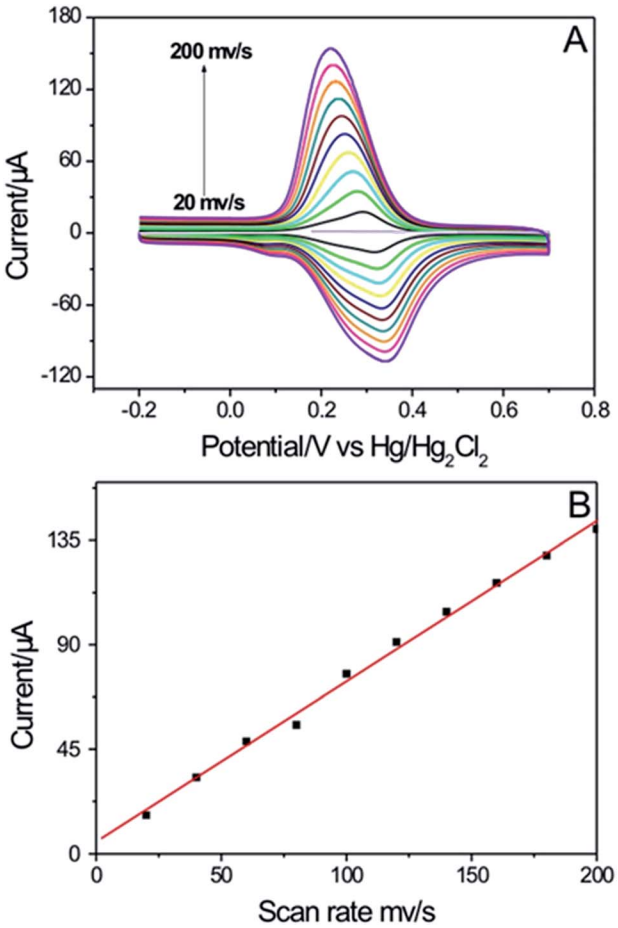

Fig. 8 (A) CVs of the integrated HPG electrode in 10^{-4} M $Fe(CN)_6^{3-}$ containing 0.1 M KCl at a scan rate ranging from 20 to 200 mV s^{-1}. (B) The plot of peak current *versus* scan rates.

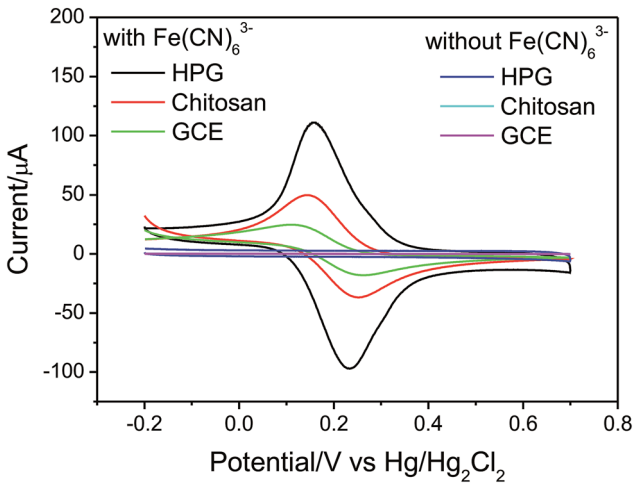

Fig. 7 Cyclic voltammograms of HPG electrode, chitosan electrode and bare GCE in the presence and absence of 5 mM $Fe(CN)_6^{3-}$ in 0.1 M KCl at 20 mV s^{-1} (the magnifying image of this figure was saw in Fig. S3†).

than the other four electrodes. This result can be explained by the ideal graphitic framework of HPG. Fig. 6B shows the Nyquist plots in the range of 100 kHz to 10 mHz for different electrodes. It is well known that the diameter of the semicircle is a direct representation of the charge transfer resistance (R_{ct}).[41] Fig. 6B clearly indicates that the bare GCE has higher R_{ct} than the other four modified electrodes, which suggests that the active hierarchically porous carbons samples have lower R_{ct} values. The slope of HPG electrode was the steepest at the low-frequency region, which suggests that the HPG electrode has a lower impedance at the electrode/electrolyte interface.[41] The HPG is considered to provide not only highly porous structures for charged particle diffusion, but also graphitic structures for accelerating electrons movement, both of which contribute to better electrochemical performance. Meanwhile, the HPGS electrode, HPG-Fe electrode and HPC electrode didn't exhibit a better electrochemical performance should due to their destroyed of graphite structure, low porosity and low degree of graphitization, respectively. Therefore, HPG electrode was chose for further experiments.

The detail electrochemical features of the HPG electrode composite electrode were examined in 0.1 M KCl. As shown in

Fig. 7, in the absence of $Fe(CN)_6^{3-}$, no obvious peak was observed. In the presence of 5 mM $Fe(CN)_6^{3-}$, a pair of redox peaks of ferricyanide ion was observed. Compared with the CV of GCE, an enhancement of the peak currents was observed at chitosan electrode. This may be caused by the positively charged chitosan which could help to attract negative $Fe(CN)_6^{3-}$ ions. The redox peaks of HPG electrode were much stronger and clearer than those of the bare GCE and chitosan electrode, indicating that HPG plays the key role in increasing the electroactive surface and providing the conducting bridges for the electron transfer of $Fe(CN)_6^{3-/4-}$.

Fig. 8A shows the CVs of the integrated HPG electrode in 10^{-4} M $Fe(CN)_6^{3-}$ containing 0.1 M KCl at a scan rate ranging from 20 to 200 mV s^{-1}. The peak current increased linearly with the scan rate (Fig. 8B), suggesting that the electrode reactions of $Fe(CN)_6^{3-}$ were predominantly a surface-controlled processes on the HPG electrode.[42] The surface excess of $Fe(CN)_6^{3-}$ is 1.153×10^{-9} mol cm^{-2} (see in Fig. S4†).

Fig. 9A shows the peak-current values of HPG electrode in different $Fe(CN)_6^{3-}$ concentrations in DPV method. The plot of peak current *versus* concentration exhibited good linearity in the range of 1–10 nM, with a correlation coefficient of 0.998 (see in Fig. 9B). This result indicates the HPG electrode has a high sensitivity to electroactive species.

The above electrochemical properties of HPG electrode means it has the potential to be used as the chemical sensor for the electroactive NO_2^- ions in drinking water. Therefore, the performance of the HPG electrode compared with chitosan electrode and bare GCE was examined in 0.1 M PBS buffer solution (pH = 7). As shown in Fig. 10, there is no peak obtained in the absence of NO_2^-. In the presence of 10 mM analytes, only HPG exhibited a large current which reveals the as-prepared HPG electrode has a good electrochemical response to the NO_2^- in water. Besides the peak current was proportional to scan rate in the CV plot, suggesting that the electrode reactions of nitrite were predominantly a surface-controlled processes on the HPG electrode (see in Fig. S6†).[42] The surface excess of NO_2^- is 9.844×10^{-9} mol cm^{-2} (see in Fig. S7†).

The Fig. 11A clearly exhibits the peak currents increase when concentrations of NO_2^- increase. Furthermore, the peak currents values also exhibited a linear dependence with the concentrations of NO_2^-. The HPG electrode showed good performances toward the detection of NO_2^- present in concentrations of 0.2–0.8 mM ($r = 0.999$, Fig. 11B) and 2–10 mM ($r = 0.996$, Fig. 11C), with a detection limit of 8.1×10^{-3} mM (S/N = 3). The excellent sensing properties of HPG electrode are due to the large specific surface area, the versatile structure and the good electrical conductivity. The developed carbon network and continuous macroporous structures will guarantee rapid transfer/diffusion of electrolyte ions throughout the entire surface area, respectively, and the large surface area and mesopores will result in a large number of active sites that attract the negatively charged ions of NO_2^-, and it is possible to accumulate NO_2^- on the electrode surfaces.

The possible interference of the presence of various organic matters and inorganic ions, which may coexist with NO_2^- in real samples, was also studied. When each 100-fold of urea, glucose,

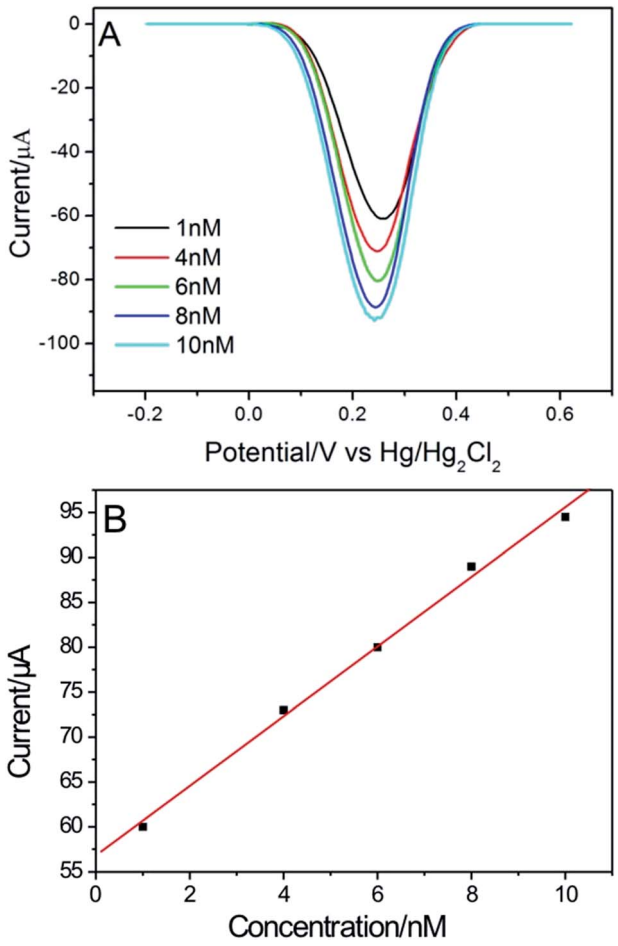

Fig. 9 (A) DPV responses of the HPG electrode to $Fe(CN)_6^{3-}$ at different concentrations. (B) The corresponding linearity curve.

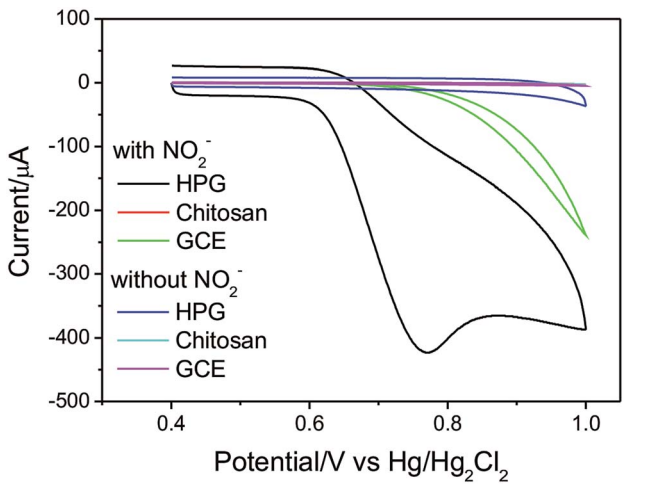

Fig. 10 Cyclic voltammograms of HPG electrode, chitosan electrode and bare GCE in the presence and absence of 10 mM NO_2^- in 0.1 M PBS buffer solution (pH = 7) at 100 mV s^{-1} (the magnifying image of this figure was saw in Fig. S5, in the ESI†).

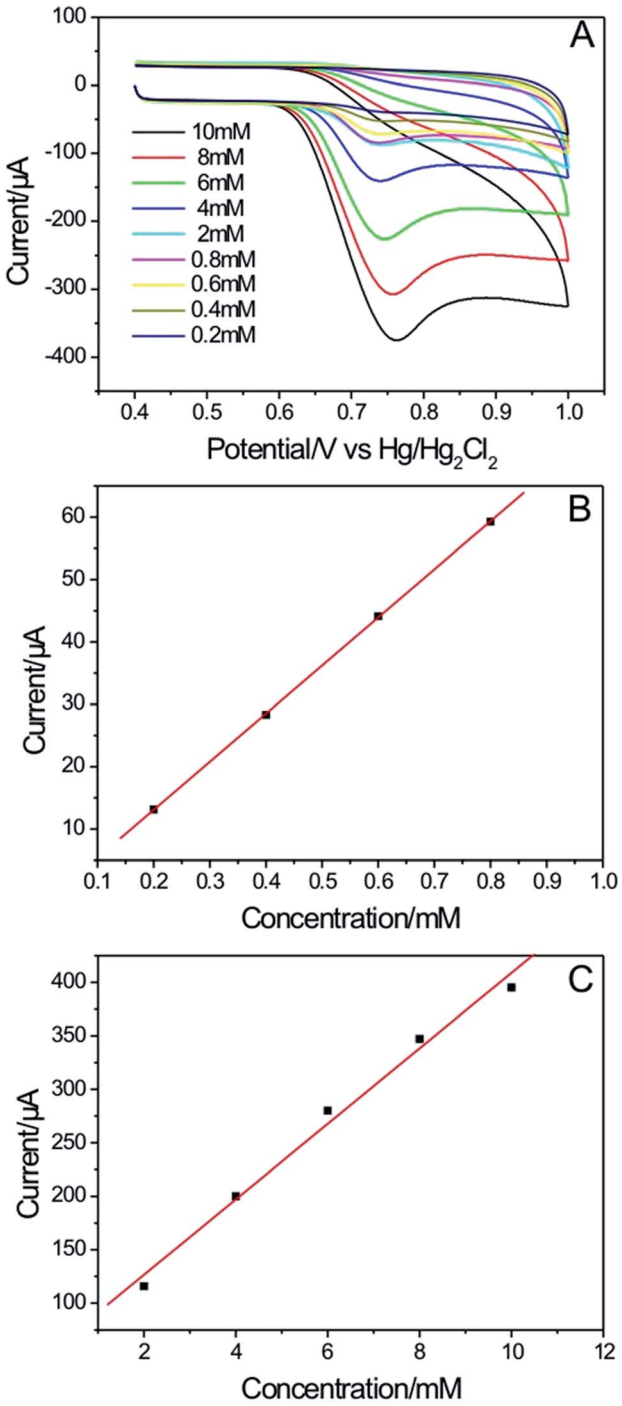

Fig. 11 (A) CV responses of the HPG electrode to NO_2^- at different concentrations. (B) The corresponding linearity curve (at concentrations ranging from 0.2–0.8 mM). (C) The corresponding linearity curve (at concentrations ranging from 2–10 mM).

KNO_3, KCl, $Mg(NO_3)_2$, and K_2SO_4 were added into the pH 7.0 PBS solution, the responses of HPG electrodes to NO_2^- were not affected. It demonstrates that those possibly coexisted chemicals had no influence on determination of NO_2^-, with deviations of <2%. The repeatability of the electrode was investigated by repetitively determining 3.5 mM NO_2^-. The relative standard deviation (RSD) of peak currents was 5.6% (n = 10). The response sensitivity retained a value of 92% over 6 weeks at room temperature. The three independently prepared electrodes to determine 5 mM nitrite showed an acceptable reproducibility with an RSD of 4%. These results suggest that the integrated HPG electrode is stable and repeatable to selectively detect nitrites. To explore the possible application of the proposed method, the experiments were studied in various drinkable water samples (tap water, lake water, mineral water, juice and pure milk). The results are shown in Table 2, and the recoveries ranged between 92% and 104%. Therefore, the developed sensor could be preliminarily applied to determine nitrite in environmental samples.

Table 2 Detection of practical samples

Real sample	Added (mM)	Found (mM)	Recovery (%)
Tap water	5	4.92	98.4
	0.5	0.48	96
Lake water	5	4.73	94.6
	0.5	0.48	96
Mineral water	5	5.20	104
	0.5	0.51	102
Juice	5	5.10	102
	0.5	0.46	92
Pure milk	5	5.09	101.8
	0.5	0.47	94

Compared with other reported electrodes, although the detection limit of the HPG electrode is not very low, it is lower than the national life table-water standard of China and could determine whether the quality of water reaches the standard (Table S1†). Meanwhile, the HPG is cheaper and easier to be get than carbon nanotube and graphene oxide. In addition, as an electrochemical sensor, the HPG electrode had a significant response for detecting nitrite in drinkable water (tap water, lake water, mineral water, juice and pure milk). The results confirmed that the fabricated nitrite sensor can be used for sensitive determination of nitrite in real samples.

Conclusions

In summary, we have prepared series of hierarchically porous carbon materials by template method and investigated the electrochemical performances of them. The effect of surface wettability, surface area, graphitizing degree and metal catalyst residual were explored. The surface area and graphitization were found key influence factors to the electroactivity of the researched porous materials. The HPG, which had a relatively large surface area, ideal interconnected porous structure and the high graphitizing degree, showed the best performance in all porous carbon materials. In addition, as an electrochemical sensor, the HPG electrode had significant response for detecting nitrite in drinkable water. The detection limit was as low as 8.1×10^{-3} mM. More than that, the electrochemical behavior of HPG electrode was stable during time and highly repeatable. The possibility of practical application of HPG was confirmed by

successfully determining nitrite in different drinkable water. These exhibit that the HPG is an excellent material for the construction of electrochemical sensors.

Acknowledgements

This work was supported by the National Natural Science Foundation of China (21107008, 21473019, 51273030) and the Fundamental Research Funds for the Central Universities (DUT14ZD217, DUT15LK29).

Notes and references

1 S. J. Yang, T. Kim, J. H. Im, Y. S. Kim, K. Lee, H. Jung and C. R. Park, *Chem. Mater.*, 2012, **24**(3), 464–470.
2 Y. S. Hu, P. Adelhelm, B. M. Smarsly, S. Hore, M. Antonietti and J. Maier, *Adv. Funct. Mater.*, 2007, **17**(12), 1873–1878.
3 T. C. Chou, R. A. Doong, C. C. Hu, B. Zhang and D. S. Su, *ChemSusChem*, 2014, **7**(3), 841–847.
4 L. Zhao, L. Z. Fan, M. Q. Zhou, H. Guan, S. Qiao, M. Antonietti and M. M. Titirici, *Adv. Mater.*, 2010, **22**(45), 5202–5206.
5 J. Xu, K. Wang, S. Z. Zu, B. H. Han and Z. Wei, *ACS Nano*, 2010, **4**(9), 5019–5026.
6 S. Tao, Z. Shi, G. Li and P. Li, *ChemPhysChem*, 2006, **7**(9), 1902–1905.
7 E. Frackowiak and F. Beguin, *Carbon*, 2001, **39**(6), 937–950.
8 A. Burke, *J. Power Sources*, 2000, **91**(1), 37–50.
9 S. L. Candelaria, Y. Shao, W. Zhou, X. Li, J. Xiao, J. G. Zhang, Y. Wang, J. Liu, J. Li and G. Cao, *Nano Energy*, 2012, **1**(2), 195–220.
10 A. Pandolfo and A. Hollenkamp, *J. Power Sources*, 2006, **157**(1), 11–27.
11 L. Zhang and L. X. Zhao, *Chem. Soc. Rev.*, 2009, **38**(9), 2520–2531.
12 H. Zanin, E. Saito, H. Ceragioli, V. Baranauskas and E. Corat, *Mater. Res. Bull.*, 2014, **49**, 487–493.
13 R. S. Borges, A. L. M. Reddy, M. T. F. Rodrigues, H. Gullapalli, K. Balakrishnan, G. G. Silva and P. M. Ajayan, *Sci. Rep.*, 2013, **3**, 2572.
14 P. Chen and R. L. McCreery, *Anal. Chem.*, 1996, **68**(22), 3958–3965.
15 J. M. Nugent, K. S. V. Santhanam, A. Rubio and P. M. Ajayan, *Nano Lett.*, 2001, **1**(2), 87–91.
16 M. C. Liu, L. B. Kong, P. Zhang, Y. C. Luo and L. Kang, *Electrochim. Acta*, 2012, **60**, 443–448.
17 V. Ruiz, C. Blanco, R. Santamaría, J. Ramos Fernández, M. Martínez Escandell, A. Sepúlveda Escribano and F. Rodríguez Reinoso, *Carbon*, 2009, **47**(1), 195–200.
18 M. Clark, M. O. Davies, E. Yeager and F. Hovorka, *J. Electrochem. Soc.*, 1956, **103**(9), 203.
19 Y. Li, Z. Y. Fu and B. L. Su, *Adv. Funct. Mater.*, 2012, **22**(22), 4634–4667.
20 Y. Li, Z. Li and P. K. Shen, *Adv. Mater.*, 2013, **25**(17), 2474–2480.
21 Y. Lv, L. Gan, M. Liu, W. Xiong, Z. Xu, D. Zhu and D. S. Wright, *J. Power Sources*, 2012, **209**, 152–157.
22 P. K. Chu and L. Li, *Mater. Chem. Phys.*, 2006, **96**(2), 253–277.
23 Y. Sun, X. He, J. Ji, M. Jia, Z. Wang and X. Sun, *Talanta*, 2015, **141**, 300–306.
24 S. Shahrokhian, M. Azimzadeh and M. K. Amini, *Mater. Sci. Eng., C*, 2015, **53**, 134–141.
25 V. Kumar, M. Shorie, A. K. Ganguli and P. Sabherwal, *Biosens. Bioelectron.*, 2015, **72**, 56–60.
26 B. Li, G. Pan, N. D. Avent, R. B. Lowry, T. E. Madgett and P. L. Waines, *Biosens. Bioelectron.*, 2015, **72**, 313–319.
27 K. S. Kim, J. R. Jang, W. S. Choe and P. J. Yoo, *Biosens. Bioelectron.*, 2015, **71**, 214–221.
28 A. Fei, Q. Liu, J. Huan, J. Qian, X. Dong, B. Qiu, H. Mao and K. Wang, *Biosens. Bioelectron.*, 2015, **70**, 122–129.
29 S. Tao, Y. Wang, D. Shi, Y. An, J. Qiu, Y. Zhao, Y. Cao and X. Zhang, *J. Mater. Chem. A*, 2014, **2**(32), 12785–12791.
30 D. Wei, Y. Liu and Y. Wang, *Nano Lett.*, 2009, **9**(5), 1752–1758.
31 B. R. Kozub, N. V. Rees and R. G. Compton, *Sens. Actuators, B*, 2010, **143**(2), 539–546.
32 W. Lijinsky, E. Conrad and R. van de Bogart, *Nature*, 1972, **239**, 165–167.
33 S. S. Mirvish, *Cancer Lett.*, 1995, **93**(1), 17–48.
34 T. Zhang, H. Fan and Q. Jin, *Talanta*, 2010, **81**(1), 95–99.
35 L. Zhao, H. Xu, H. Li and J. Chen, *Occup. Health*, 2010, **26**(20), 2315.
36 Y. R. Liang, F. X. Liang, D. C. Wu, Z. H. Li, F. Xu and R. W. Fu, *Phys. Chem. Chem. Phys.*, 2011, **13**(19), 8852–8856.
37 T. Amatani, K. Nakanishi, K. Hirao and T. Kodaira, *Chem. Mater.*, 2005, **17**(8), 2114–2119.
38 K. Sonnenburg, P. Adelhelm, M. Antonietti, B. Smarsly, R. Nöske and P. Strauch, *Phys. Chem. Chem. Phys.*, 2006, **8**(30), 3561–3566.
39 J. Li, R. Lu, B. Dou, C. Ma, Q. Hu, Y. Liang, F. Wu, S. Qiao and Z. Hao, *Environ. Sci. Technol.*, 2012, **46**(22), 12648–12654.
40 G. Wang, J. Yang, J. Park, X. Gou, B. Wang, H. Liu and J. Yao, *J. Phys. Chem. C*, 2008, **112**(22), 8192–8195.
41 L. Strašák, J. Dvořák, S. Hasoň and V. Vetterl, *Bioelectrochemistry*, 2002, **56**(1), 37–41.
42 L. Wang, Q. Zhang, S. Chen, F. Xu, S. Chen, J. Jia, H. Tan, H. Hou and Y. Song, *Anal. Chem.*, 2014, **86**(3), 1414–1421.